2016-01

Experimental Implementation of Riemann--Stieltjes Optimal Control for Agile Imaging Satellites

Karpenko, Mark

Engineering Notes

Experimental Implementation of Riemann–Stieltjes Optimal Control for Agile Imaging Satellites

Mark Karpenko* and Ronald J. Proulx†
Naval Postgraduate School, Monterey, California 93943

DOI: 10.2514/1.G001325

I. Introduction

INCREASING the agility of an imaging satellite allows the slew time between images to be reduced and can significantly increase the number of collections in a given access window. One approach for enhancing agility, without the need for hardware change, is to employ optimal control theory to design shortest-time maneuvers that satisfy all the relevant practical and operational constraints. Because standard optimal control solutions provide an open-loop control trajectory based on a nominal model of the plant, open-loop implementation of the optimal control is not operationally feasible for imaging systems. This is because tight tolerances on pointing accuracy are required to perform the imaging task. Therefore, even if the dynamics of the satellite are known with a good degree of accuracy, feedback is still needed to ensure that requirements on pointing accuracy can be met.

For a reaction wheel spacecraft, the feedback implementation of the shortest-time maneuvers can be accomplished relatively easily by using the attitude control law to track the optimal attitude trajectories. This approach has been successfully demonstrated in flight tests onboard NASA's Transition Region and Coronal Explorer [1]. A significant challenge in migrating this implementation concept to imaging systems that use control moment gyroscopes (CMGs) is the fact that the feedback law for a CMG momentum control system includes a steering algorithm that may become singular for certain combinations of CMG gimbal angles. Therefore, when the optimal control is implemented in the closed-loop, unpredictable interactions between the nominal open-loop trajectories and the steering law can cause the system to fail to meet its objective. For example, the control action of the feedback law can perturb the CMGs toward a singular state even though the optimal gimbal trajectories are far from singularities.

One of the few papers to study the implementation of closed-loop optimal slew maneuvers for CMG systems is the work of McFarland et al. [2], who implemented real-time optimal control for a small CMG testbed located at the United States Air Force Institute of Technology. In this approach, the optimal gimbal rates can be fed forward to the CMGs, thereby sidestepping the need for a traditional

steering law. The practical challenge with real-time optimal control is that an algorithm must be embedded as part of the flight control software. While the technology readily exists for doing so (see [3]), the costs associated with flight software changes typically preclude the industry from adopting this "risky" approach.

In response to the current state of the art, this note proposes a new approach for enhancing the agility of a CMG satellite that can be implemented using conventional attitude control architectures and without the need to change the flight hardware. It is shown that it is wpossible to account for the perturbations introduced due to feedback *a priori*, during maneuver design, through the development of a tychastic [4] optimal control constraint. This constraint allows the control authority of the CMG array to be maintained despite significant uncertainty in the evolution of the gimbal angles from their nominal trajectories. The approach thus provides a margin for feedback, which is calculable in a statistical sense. The resulting nonstandard optimal control problems are solved using the Riemann–Stieltjes optimal control framework [5–7]. Experimental results from a series of tests performed on Honeywell's momentum control system testbed are presented for both nominal and off-nominal operating conditions to illustrate the feasibility of implementing the approach on a practical CMG attitude control system.

II. CMG Attitude Control

A. System Model

The standard equation expressing the rotational dynamics of a CMG spacecraft is given by [8]:

$$J\dot{\omega} + \omega \times J\omega + \omega \times h + \dot{h} = 0 \qquad (1)$$

where matrix J is the inertia tensor of the spacecraft including the CMGs, ω is the vector of spacecraft angular rates, and h is the momentum vector of the CMG array expressed in the body frame.

The momentum vector of each CMG h_i can be expressed with respect to a fixed frame, p, through a transformation of the form (see Fig. 1)

$$h_i = J_s \Omega_s \begin{bmatrix} \cos(\alpha_i)\cos(\beta)\sin(\delta_i) + \sin(\alpha_i)\cos(\delta_i) \\ -\sin(\alpha_i)\cos(\beta)\sin(\delta_i) + \cos(\alpha_i)\cos(\delta_i) \\ \sin(\beta)\sin(\delta_i) \end{bmatrix} \qquad (2)$$

where J_s is the rotor inertia about the spin axis and Ω_s is the rotor angular rate. Angles α_i and β denote the base circle spacing angle and the fixed pyramid skew angle, respectively. Δ_i is the CMG gimbal angle

The torques expressed in frame p are

$$\sum_{i=1}^{n} \dot{h}_i = J_s \Omega_s A(\Delta)\dot{\Delta} \qquad (3)$$

where $\Delta = [\delta_1, \delta_2, \ldots, \delta_n]^T$ and the columns of matrix $A(\Delta) = [a_1(\delta_1)|a_2(\delta_2)| \cdots a_n(\delta_n)]$ are obtained by differentiating the individual CMG momentum vectors with respect to time and separating the resulting $\dot{\delta}$ terms. For example, differentiating Eq. (2) and separating $\dot{\delta}$ gives the torque due to CMG i as

$$\dot{h}_i = J_s \Omega_s a_i \dot{\delta}_i = J_s \Omega_s \begin{bmatrix} \cos(\alpha_i)\cos(\beta)\cos(\delta_i) - \sin(\alpha_i)\sin(\delta_i) \\ -\sin(\alpha_i)\cos(\beta)\cos(\delta_i) - \cos(\alpha_i)\sin(\delta_i) \\ \sin(\beta)\cos(\delta_i) \end{bmatrix} \dot{\delta}_i \qquad (4)$$

Using the above definitions for the CMG angular momentum vector and its time derivative, and by representing the attitude
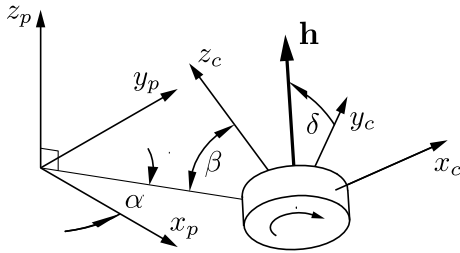
Fig. 1   Momentum vector h of a CMG in relation to a fixed frame, p.

kinematics using quaternions, a system of nonlinear ordinary differential equations describing the dynamics of the spacecraft can be written as

$$\dot{x} = \begin{bmatrix} \dot{q} \\ \dot{q}_4 \\ \dot{\omega} \\ \dot{\Delta} \end{bmatrix} = \begin{bmatrix} \frac{1}{2}(q_4\omega - \omega \times q) \\ -\frac{1}{2}\omega^T q \\ J^{-1}\left\{-\omega \times \left(J\omega + R_p \sum_{i=1}^{n} h_i\right) - J_s\Omega_s R_p A(\Delta)u\right\} \\ u \end{bmatrix}$$

$$(5)$$

where R_p is a rotation matrix relating the CMG pallet frame to the spacecraft body frame.

B.   Feedback Control Architecture

The block diagram of a feedback architecture that can be used to implement optimal attitude maneuvers is shown in Fig. 2. The feedback system comprises an attitude estimator, a feedback law, and a CMG steering law. The feedback law provides a torque command, τ_c, in the spacecraft body frame to drive the error between the commanded optimal attitude and rate, $q_c(t)$ and $\omega_c(t)$, and the estimated attitude and rate, $\hat{q}$ and $\hat{\omega}$, to zero. The role of the steering law is to allocate the feedback torque among the individual CMGs in terms of a set of corrective gimbal rate commands, $\dot{\Delta}_{\text{fb}}$. Because the open-loop control allocation problem is solved as part of the optimal control problem [9], gimbal rate feedforward commands, $\dot{\Delta}_c$, are also available to drive the CMG gimbals directly. If the nominal plant model closely matches the actual satellite dynamics, $\dot{\Delta}_{\text{fb}}(t) \approx 0$ and the maneuver implementation will be successful. In practice, however, parametric and other uncertainties, for example, gimbal angle drift, cause $\dot{\Delta}_{\text{fb}}(t) \neq 0$ due to the discrepancy between the modeled and actual rotational dynamics. In this case, the feedback implementation of the optimal control solution can fail due to the introduction of feedback commands that drive the CMG gimbals away from the optimal control solution. The failure is manifest as a reduction in the control authority of the CMG array, possibly to zero, leading to a temporary loss of control of the satellite. This problem can prevent successful implementation of optimal control solutions on practical systems. The Riemann–Stieltjes optimal control framework described in the next section provides a mechanism for ameliorating this issue. The key idea is the formulation of a nonstandard optimal control problem that provides different gimbal angle trajectories than a standard optimal control solution. These new gimbal angle trajectories desensitize the variation in the CMG singularity index (a measure of CMG control authority) to large perturbations in the orientations of the gimbals that can occur due to feedback. Using this framework, feedback authority can therefore be purposefully

reserved to counteract the effects of system uncertainties so that the optimal control solution can be successfully implemented in a feedback setting.

III.   Application of Riemann–Stieltjes Optimal Control

A standard formulation of the point-to-point maneuver design problem for a CMG spacecraft can be expressed as [9–11]

$$P_{\text{STD}}(x_0, x_f): \begin{cases} \text{Minimize} & J[x(\cdot), u(\cdot), t] = t_f - t_0 \\ \text{Subject to} & \dot{x} = f(x, u, t) \\ & x_0 = [q(t_0), \omega(t_0), \Delta(t_0)]^T \\ & x_f = [q(t_f), \omega(t_f), \Delta(t_f)]^T \\ & h(x, u, t) \leq 0 \end{cases}$$

$$(6)$$

where the symbol $P_{\text{STD}}(x_0, x_f)$ is used to emphasize that the boundary conditions on the problem change between individual point-to-point maneuvers. For satellite imaging problems, an additional complication arises because the boundary conditions are dependent on the specific values of t_0 and t_f. This is a result of the relative motion between the satellite and the coordinates of area to be imaged. The correct boundary conditions at any instant in time must therefore be embedded as part of the optimal control problem formulation. In addition, the momentum state of the CMG array at the beginning and end of each maneuver must be consistent with the initial and final satellite angular rates (which are generally nonzero for Earth imaging applications) and account for any environmental disturbances accumulated during the maneuver. To design maneuvers that can be implemented on a real spacecraft system, it is also necessary to define additional constraints on the states and/or controls, such as the quaternion norm condition and the conservation of angular momentum. This is accomplished by defining the appropriate constraints $h(x, u, t) \leq 0$ for the optimal control problem. The solution of problem P_{STD} Eq. (6) gives the state-control function pair $t \rightarrow (x, u)$, where $u = \dot{\Delta}_c$, that drives the satellite having dynamics given by Eq. (5), as quickly as possible between the operationally specified boundary conditions.

For feedback implementation of optimal CMG slews, it is necessary to additionally ensure that some margin of control authority can be reserved for feedback. One practical measure of the available margin of a CMG array is the singularity index [12] given by

$$\mathcal{S}(\Delta) = \sqrt{\det[A(\Delta)A^T(\Delta)]}$$

$$(7)$$

A pragmatic approach for developing a feedback margin is to introduce the constraint $h_{\mathcal{S}}(x, u, t) := \mathcal{S}(\Delta(t)) \geq \mathcal{S}_{\min}$, where $\mathcal{S}_{\min}$ is some appropriately chosen nonzero value. The inequality $\mathcal{S}(\Delta(t)) \geq \mathcal{S}_{\min}$ guarantees that the CMG array can be maintained in a steerable state about the nominal control trajectory. Assume now that, due to the effects of feedback, the optimal control trajectory $u(t) = \dot{\Delta}_c(t)$ is perturbed by an amount $\dot{\Delta}_{\text{fb}}(t)$, so that the gimbal rate commands seen by the CMGs are $\dot{\Delta}(t) = \dot{\Delta}_c(t) + \dot{\Delta}_{\text{fb}}(t)$. The resulting evolution of the gimbal angles is $\Delta(t) = \int_{t_0}^{t} \dot{\Delta}_c(t)\,dt + \int_{t_0}^{t} \dot{\Delta}_{\text{fb}}(t)\,dt \neq \int_{t_0}^{t} \dot{\Delta}_c(t)\,dt$. In practice, the exact values of $\dot{\Delta}_{\text{fb}}(t)$ are not known *a priori* and may become quite large. Thus, the actual values of $\mathcal{S}(\Delta(t))$ can deviate significantly from nominal. As a consequence, the action of the feedback loop may cause the violation of constraint $\mathcal{S}(\Delta(t)) \geq$
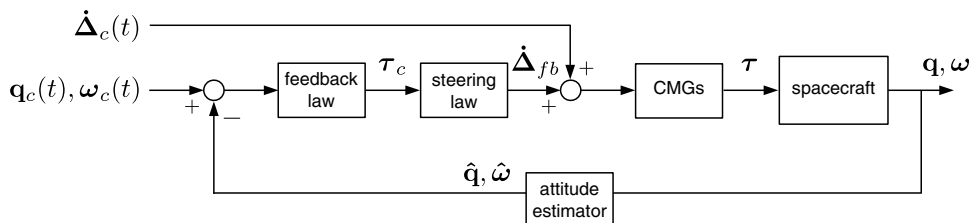

Fig. 2   Control system block diagram for optimal attitude control of a CMG spacecraft.

$\mathcal{S}_{\min}$ when the maneuver is implemented. In fact, as will be seen later, the condition $\mathcal{S}(\mathbf{\Delta}(t)) \ll \mathcal{S}_{\min}$ can occur and cause the steering to become singular. Rather than reserving a larger margin on control authority by increasing the value of $\mathcal{S}_{\min}$ (this can increase maneuver times to the point of operational infeasibility), we employ the newly developed framework of Riemann–Stieltjes optimal control [5–7] and implement a tychastic constraint on $\mathcal{S}(\mathbf{\Delta}(t))$.

To construct the Riemann–Stieltjes optimal control problem for agile CMG maneuvering, it is useful to appreciate the fact that, in the present application, feedback is available to accommodate system uncertainties. This allows the original Riemann–Stieltjes optimal control problem [5], which was developed for uncertainty management in an open-loop setting, to be significantly reduced in scope. Instead of finding a single control history, $\mathbf{\Delta}_c^*(t)$, that drives the uncertain satellite dynamics to the prescribed terminal state in the open loop, all that is necessary is to ensure that a margin for feedback can be made available by managing the configuration of the CMGs along the optimal trajectory. This can be done by properly constraining the allowable variation in $\mathcal{S}(\mathbf{\Delta}(t))$.

While the precise nature of $\dot{\mathbf{\Delta}}_{\mathrm{fb}}(t)$ resulting from the feedback implementation of a solution to Eq. (6) is impossible to know in advance, the perturbation induced by steering about the nominal trajectory can be approximated. For example, it is possible to model the value of the instantaneous gimbal angle for each CMG using a Normal distribution, $\mathcal{N}(\mu_i, \sigma^2)$, where μ_i is the nominal (mean) value of the gimbal angle for CMG i and σ is the presumed standard deviation from the mean (the statistical off-nominal perturbation). At each instant in time, the statistics on $\mathcal{S}(\mathbf{\Delta}(t))$ are computed as a multidimensional Riemann–Stieltjes integral. For example, the expected value of $\mathcal{S}(\mathbf{\Delta}(t))$ may be computed as

$$E[\mathcal{S}(\mathbf{\Delta}(t))] = \int \int \cdots \int \mathcal{S}(\delta_1(t), \delta_2(t), \ldots, \delta_n(t))$$
$$\mathrm{d}\Phi\left(\frac{\delta_1(t) - \mu_1(t)}{\sigma^2}\right) \mathrm{d}\Phi\left(\frac{\delta_2(t) - \mu_2(t)}{\sigma^2}\right) \mathrm{d}\Phi\left(\frac{\delta_n(t) - \mu_n(t)}{\sigma^2}\right) \quad (8)$$

Equation (8) allows the mean value of the uncertain CMG singularity index to be computed along the nominal gimbal angle trajectories. Because Eq. (7) is a nonlinear equation, we note that the values of $E[\mathcal{S}(\mathbf{\Delta})]$ are generally not the same as the values $\mathcal{S}(\mathbf{\Delta}_{\mathrm{nom}})$. The following constraint on the CMG singularity index may thus be used in the Riemann–Stieltjes optimal control problem formulation:

$$h_1(\mathbf{x}, \mathbf{u}, t) := E[\mathcal{S}(\mathbf{\Delta}(t))] \geq \mathcal{S}_{\min} \quad (9)$$

To illustrate the utility of constraint (9), Fig. 3 provides typical probability distributions (PDs) of the CMG singularity index of an array of four CMGs. An example bound $\mathcal{S}_{\min} = 0.5$ on constraint (9) is also marked on the plot. The results were obtained from a
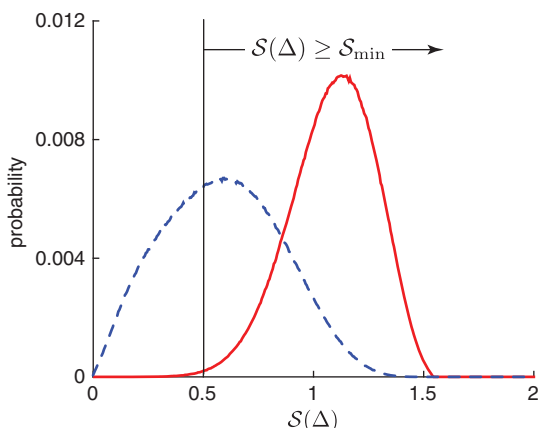

Fig. 3 **Probability distributions of the singularity index for two example gimbal angle configurations. Solid line, possible CMG configuration at the beginning of a slew; dashed line, possible CMG configuration during an agile slew.**

Monte Carlo analysis with an assumed gimbal angle uncertainty of $\sigma = 10°$. Two cases are given. In the first, the nominal gimbal angles correspond to a zero-net momentum condition (a typical nominal configuration at the beginning of a maneuver). In the second case, the gimbal angles correspond to a situation where a large momentum has been transferred to the satellite by the CMGs (a possible configuration encountered during an agile slew). Referring to the variation in the CMG singularity index for the zero-net momentum condition (solid line), it is seen that only the tail of the PD lies below $\mathcal{S}_{\min} = 0.5$. In this case, the probability of violating the specified constraint (9) is quite small, $\Pr\{\mathcal{S}(\mathbf{\Delta}) < 0.5\} \approx 0.003$. For the example CMG configuration encountered during the slew (dashed line), the constraint $E[\mathcal{S}(\mathbf{\Delta}(t))] \geq 0.5$ is also satisfied. Yet, a large portion of the PD lies below the specified bound, that is, $\Pr\{\mathcal{S}(\mathbf{\Delta}) < 0.5\} \approx 0.38$. As a consequence, if this particular set of gimbal angles was to form part of an optimal control trajectory, there is a reasonably good chance that constraint (9) would be violated due to the action of the feedback controller. Furthermore, in some cases, the singularity index is observed to become zero, indicating that a singular configuration of the CMGs is possible if the off-nominal perturbations become large enough. This condition could lead to the failure of the maneuver.

In light of the observations described above, construction of a different constraint appears to be necessary for operational success. Because the goal is to ensure that some margin on control can always be retained for feedback, it would be more appropriate to build a constraint that ensures that $\Pr\{\mathcal{S}(\mathbf{\Delta}) < \mathcal{S}_{\min}\}$ is as small as possible. One approach for providing a (statistically) guaranteed margin on feedback is to formulate a constraint in which $\Pr\{\mathcal{S}(\mathbf{\Delta}) \leq \mu_{\mathcal{S}} - 3\sigma_{\mathcal{S}}\} < \epsilon$, where subscript $\mathcal{S}$ is used to refer to the statistics of $\mathcal{S}(\mathbf{\Delta})$ and ϵ is an appropriately chosen small number. The relevant constraint on the CMG gimbal angles then becomes

$$h_2(\mathbf{x}, \mathbf{u}, t) := E[\mathcal{S}(\mathbf{\Delta}(t))] - 3\{E[(\mathcal{S}(\mathbf{\Delta}(t)) - E[\mathcal{S}(\mathbf{\Delta}(t))]^2]\}^{1/2} \geq \mathcal{S}_{\min} \quad (10)$$

Because Eq. (10) constrains the 3σ values of the mean singularity index to lie above the lower bound $\mathcal{S}_{\min}$, the constraint automatically satisfies (9). In the context of Fig. 3, satisfying Eq. (10) implies that a new set of nominal gimbal angles should be found to shift the PD of the troublesome CMG configuration to the right as illustrated in Fig. 4. Clearly, finding the gimbal angles that satisfy Eq. (10) involves the computation of higher-order expectations. The resulting Riemann–Stieltjes optimal control problem formulation for agile CMG maneuvering may now be written as

$$P_{\mathrm{RS}}(X_0, X_f): \begin{cases} \text{Minimize } J[X(\cdot), \mathbf{u}(\cdot), t] = t_f - t_0 \\ \text{Subject to } \dot{\mathbf{x}}_1 = \mathbf{f}(\mathbf{x}_1, \mathbf{u}, t) \\ \qquad\quad \dot{\mathbf{x}}_2 = \mathbf{f}(\mathbf{x}_2, \mathbf{u}, t) \\ \qquad\quad \vdots \\ \qquad\quad \dot{\mathbf{x}}_N = \mathbf{f}(\mathbf{x}_N, \mathbf{u}, t) \\ \qquad\quad \mathbf{x}_1^0 = [\mathbf{q}(t_0), \boldsymbol{\omega}(t_0), \mathbf{\Delta}_1(t_0)]^T \\ \qquad\quad \mathbf{x}_2^0 = [\mathbf{q}(t_0), \boldsymbol{\omega}(t_0), \mathbf{\Delta}_2(t_0)]^T \\ \qquad\quad \vdots \\ \qquad\quad \mathbf{x}_N^0 = [\mathbf{q}(t_0), \boldsymbol{\omega}(t_0), \mathbf{\Delta}_N(t_0)]^T \\ \qquad\quad \mathbf{x}_1^f = [\mathbf{q}(t_f), \boldsymbol{\omega}(t_f), \mathbf{\Delta}_1(t_f)]^T \\ \qquad\quad \mathbf{\Delta}_i(t_0) \sim \mathcal{N}(\mathbf{\Delta}_{\mathrm{nom}}(t_0), \sigma^2 \mathbf{I}_{4 \times 4}) \\ \qquad\quad \mathcal{S}_{\min} \leq E[\mathcal{S}(\mathbf{\Delta}(t))] - 3\{E[\mathcal{S}(\mathbf{\Delta}(t)) - E[\mathcal{S}(\mathbf{\Delta}(t))]^2]\}^{1/2} \\ \qquad\quad \mathbf{h}(\mathbf{x}, \mathbf{u}, t) \leq 0 \end{cases}$$
$$(11)$$

In Eq. (11), the approximated effects of the perturbations due to feedback are captured as uncertainties in the gimbal angle initial conditions. The gimbal angle uncertainties have Normal distributions centered on the nominal initial conditions, each with variance σ^2. The uncertainty is propagated via copies of $\mathbf{f}(\mathbf{x}, \mathbf{u}, t)$ (see [5–7] for details) so that the expectations on the CMG singularity index may be computed over the optimal trajectory. Additional requirements on the conservation of angular momentum and the quaternion norm for each copy of $\mathbf{f}(\mathbf{x}, \mathbf{u}, t)$ are embodied in the additional constraints
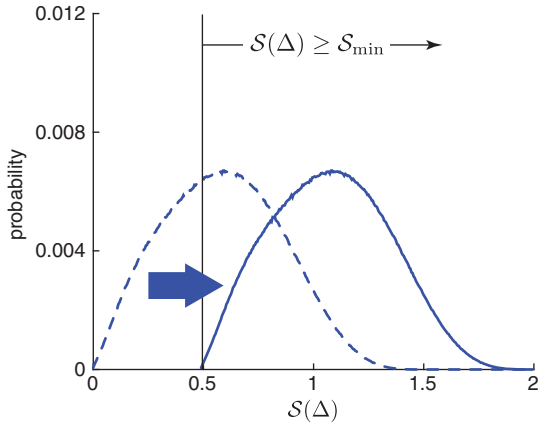
Fig. 4 Illustrating the satisfaction of constraint (10) by finding a new set of nominal gimbal angles that shifts the probability distribution to the right.

Fig. 5 Honeywell's momentum control system testbed outfitted with the Air Force Research Laboratory's miniature momentum control system.

Fig. 6 Traces of the satellite boresight path (solid red lines) required for successful image collection.

$h(x, u, t)$, given in (11). We note that Eq. (11) is a simplified form of the original Riemann–Stieltjes optimal control problem [5] because the end-point conditions must be satisfied for the nominal plant (denoted in Eq. (11) by subscript 1). It is not necessary to constrain the terminal states for the other copies of $f(x, u, t)$ because the feedback control will be used to correct any deviations that may occur due to the considered Δ uncertainty.

Having formulated an appropriate Riemann–Stieltjes optimal control problem, there remains the question of how many copies of $f(x, u, t)$ are required to accurately approximate the Riemann–Stieltjes integrals needed to compute the expectations. One approach is to solve the problem using pseudospectral methods [3] and Monte Carlo sampling, but a very large number of samples (greater than 1000) are generally required. To reduce the dimension of the problem, it is better to use sigma points [6,7] or hyper-pseudospectral (HS) points [5], $r = [r_1^0, r_2^0, \ldots, r_N^0]^T$ at $t = t^0$, which, along with a set of associated weights, $w = [w_1, w_2, \ldots, w_N]^T$, provide an efficient cubature formula for approximating Riemann–Stieltjes integrals of the form $\sum_{i=1}^N w_i E(r_i)$. To determine the appropriate number of discretization points for solving (11), the first n moments of the singularity index PD may be computed. Because transformation (7) is nonlinear, the benchmark moments are determined from a Monte Carlo simulation. The results are summarized in Table 1 along with the number of points used for the computation. To evaluate the second-order expectations in Eq. (10), an accurate estimate of the moments up to order two is required. Table 1 shows that this requirement can be met by using either set of HS points, but not the sigma points. To pose problem P_{RS} with the smallest number of points, the fifth-order HS points where $N = 23$ are used.

IV. Experimental Results

In this section, Riemann–Stieltjes optimal control solutions are implemented on the Honeywell momentum control system testbed, a hardware-in-the-loop satellite simulator (see Fig. 5). This ground test system is about 3000 lbs and floats on an airbearing at Honeywell's test facility near Phoenix, AZ. In the experiments, the momentum control system testbed was configured with the Air Force Research Laboratory's miniature momentum control system [13]. The laboratory e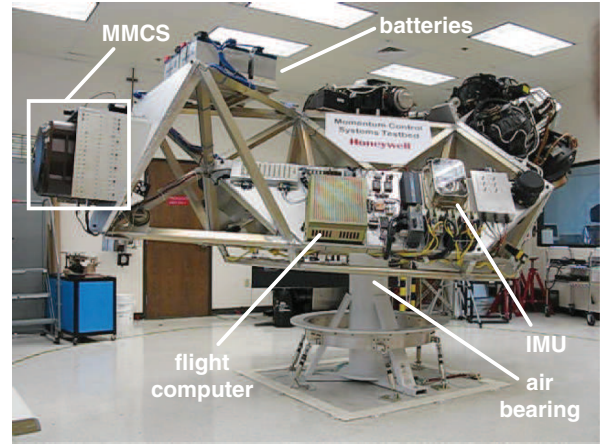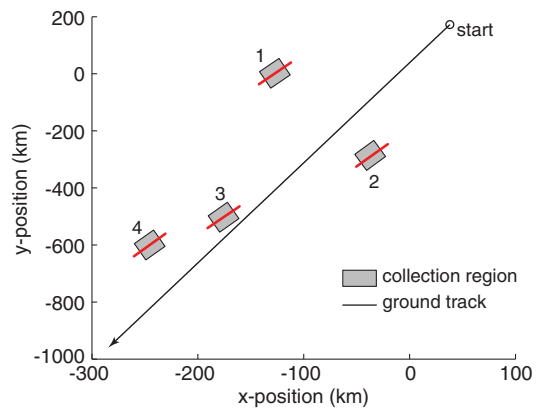xperiments mimicked the operational environment of a typical imaging satellite where the objective was to design and implement agile CMG maneuvers for point-to-point image collection.

A schematic illustrating the path of the satellite boresight (projected onto the Earth) for successful collection of four images is shown in Fig. 6. In Fig. 6, the presorted collection regions are denoted by the shaded areas. To acquire the imagery product, it is necessary for the satellite boresight to traverse through the center of each collection region as shown by the solid red lines. Note that, in this representation, it is not necessary that the boresight traces extend beyond the shaded collection regions (as is shown for clarity of the illustration). Because of the relative motion between the Earth and the satellite moving along its ground track, performing the imaging task requires careful coordination of the satellite attitude and rate so that specified tolerances on the attitude and rate tracking error during imaging can be satisfied. Meeting these stringent requirements during imaging is handled by the feedback controller. To facilitate rapid image acquisition, however, the boundary conditions on each point-to-point maneuver are made to be consistent with the attitude and rate conditions required for imaging each region. By designing the appropriate nonrest maneuvers using optimal control, the transition between the maneuvering and imaging operations can be handled in a seamless fashion.

To establish the baseline performance, a sequence of shortest-time maneuvers was designed using the standard optimal control formulation given in Eq. (6). The value of S_{min} was specified as 0.45. The designed maneuver sequence was then implemented on the hardware testbed, in the open loop, by driving the CMGs directly using the solved optimal gimbal rate commands. The results of the experiment are shown in Fig. 7. Referring to Fig. 7a, it is apparent that open-loop maneuvering allows the satellite boresight to pass roughly through the various collection regions. The pointing error due to system un-

Table 1   Estimated central moments of a typical singularity index PD

Central moment	Monte Carlo (benchmark)	Sigma points (3rd order)	HS points (5th order)	HS points (7th order)
μ_1	0	0	0	0
μ_2	$+3.68 \times 10^{-2}$	$+3.51 \times 10^{-2}$	$+3.68 \times 10^{-2}$	$+3.68 \times 10^{-2}$
μ_3	-2.71×10^{-3}	0	-2.86×10^{-3}	-2.74×10^{-3}
μ_4	$+3.95 \times 10^{-3}$	$+1.24 \times 10^{-3}$	$+3.94 \times 10^{-3}$	$+3.95 \times 10^{-3}$
N-points	10^6	8	23	52

certainties is, however, too large for successful imaging. The variation of the CMG singularity index $\mathcal{S}(\boldsymbol{\Delta}(t))$ for the open-loop implementation is shown in Fig. 7b. As is seen, the imposed constraint $\mathcal{S}(\boldsymbol{\Delta}(t)) \geq 0.45$ has not been violated. Therefore, some control authority remains so that feedback can be used in an attempt to correct the pointing errors.

In the next experiment, the shortest-time maneuvers were implemented using the feedback architecture of Fig. 2. The results of the closed-loop ground test are given in Fig. 8. Figure 8a shows that the imaging system properly collects the first image as the satellite boresight tracks the required path through the collection region. Despite the closure of the attitude loop, however, the remaining images cannot be acquired at the specified collection times. As shown by the trace of the boresight motion, the imaging sensor behaves erratically near each collection region and sometimes crosses the collection region at an angle perpendicular to the required scan direction. This implies that when the imaging sensor is activated, according the schedule stored in the satellite command buffer, the incorrect and/or blurred images will be obtained.

The reason for the incorrect behavior of the satellite is the fact that the interaction between the nominal open-loop gimbal rate commands (fed forward into the control loop) and the actions demanded by the error-driven feedback system causes the CMG array to become singular. This is clearly indicated by the time history of the CMG singularity index shown in Fig. 8b. Note that the singularities occur despite the fact that the time history of the nominal singularity index $\mathcal{S}(\boldsymbol{\Delta})_{\text{nom}}$ adheres to the imposed constraint on $\mathcal{S}_{\text{min}}$ (see Fig. 8b). During the periods of time when the CMG array is in the singular state, feedback control of the satellite is temporarily lost. While the attitude control system can eventually recover and regain control of the satellite, the singular operation of the CMGs causes the attitude to drift far enough away from the desired path that successful collection of the imagery product is generally not possible.

The sequence of agile maneuvers was next re-designed using the Riemann–Stieltjes optimal control formulation given in Eq. (11). In solving the Riemann–Stieltjes problem, it was desired to maintain the 3σ variation of the CMG singularity index above the threshold $\mathcal{S}_{\text{min}} = 0.45$ (the same value used in solving the standard optimal control problem). The standard deviation of each CMG gimbal angle from nominal was assumed to be $\sigma = 10°$. As discussed in the previous section, the satisfaction of tychastic constraint (10) ensures that only the tail of the singularity index PD will lie below the specified value of $\mathcal{S}_{\text{min}}$. The Riemann–Stieltjes optimal control therefore provides gimbal angle trajectories where the probability that of $\mathcal{S}(\boldsymbol{\Delta}) < \mathcal{S}_{\text{min}}$, due to feedback perturbations, will be small. The experimental implementation of the Riemann–Stieltjes solution is shown in Fig. 9. Referring to Fig. 9a, the imaging system is now able to acquire all four of the requested images as evidenced by the path of the boresight trace, which now passes directly through the center of each image collection region within the error tolerances required for imaging. The success of the closed-loop implementation of the Riemann–Stieltjes optimal control is a direct result of the overall improvement in the nominal CMG configuration (see $\mathcal{S}(\boldsymbol{\Delta})_{\text{nom}}$ in Fig. 9b) that is made possible by desensitizing the variation in the singularity index to large changes in the CMG gimbal angles from their nominal trajectories. The time history of the actual singularity index for the Riemann–Stieltjes optimal control experiment is observed to lie well within the 3σ envelope as shown in Fig. 9b.

Several additional experiments in which the CMG gimbals were purposefully perturbed from their nominal initial conditions were also performed to further evaluate the performance of the Riemann–Stieltjes optimal control. These tests emulate a practical operating environment where a range of off-nominal operating conditions, for example, due to gimbal angle drift, must be accommodated for mission success. The perturbations in the initial gimbal angles from nominal were selected randomly using a Normal distribution with $\mu = 0$ and $\sigma = 10°$. Both zero-net momentum and momentum-biased initial conditions were considered. In these cases, the implementation of the Riemann–Stieltjes optimal control in concert with
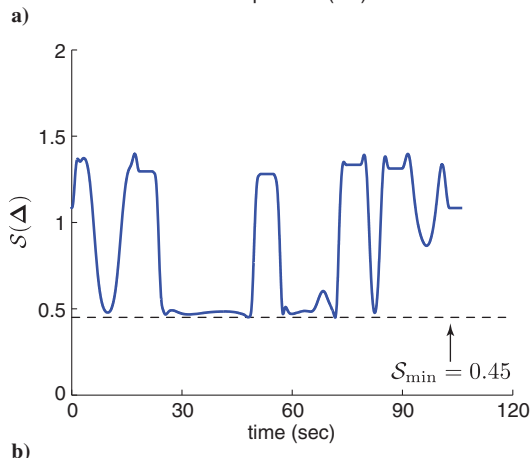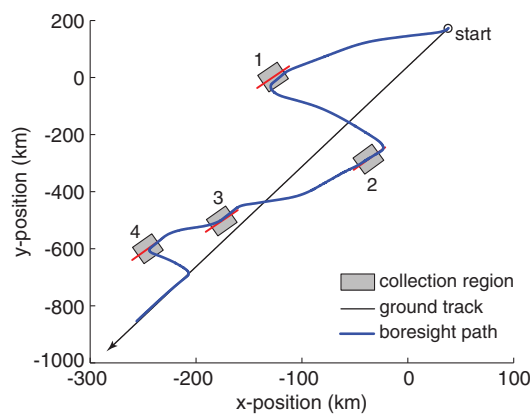

Fig. 7   Ground test results for open-loop CMG maneuvering using standard optimal control: a) boresight trace; b) CMG singularity index.
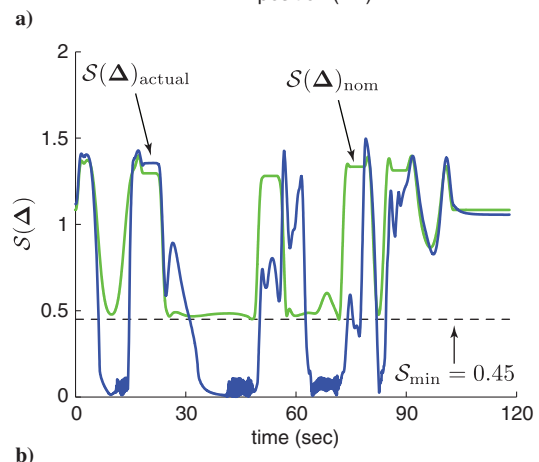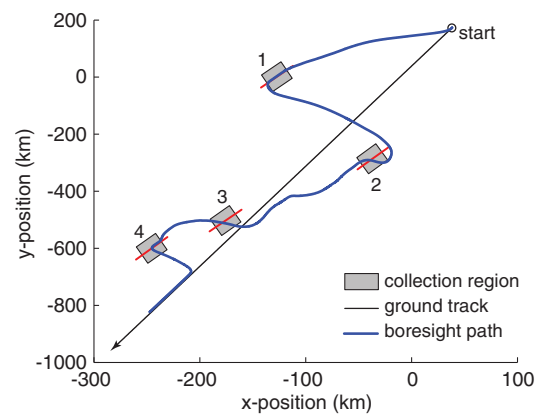

Fig 8   Ground test results for closed-loop CMG maneuvering using standard optimal control: a) boresight trace; b) nominal and actual CMG singularity index.
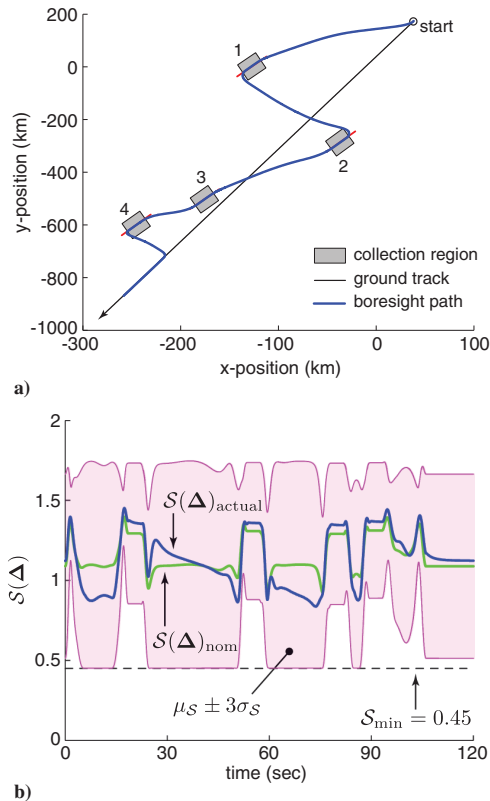
Fig. 9   Ground test results for CMG maneuvering using Riemann–Stieltjes optimal control: a) boresight trace; b) nominal and actual CMG singularity index with 3σ envelope.

the conventional feedback controller allowed the imaging process to be successfully completed despite the off-nominal perturbations. Some ground test results are presented in Fig. 10. Referring to the
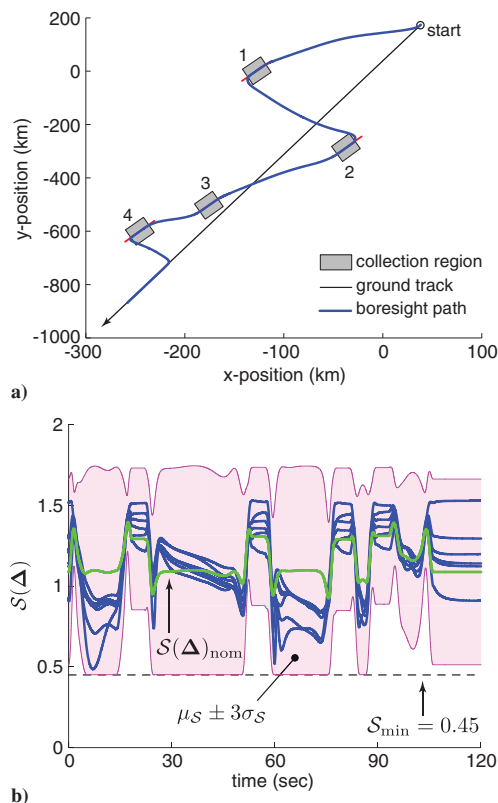
boresight traces (Fig. 10a), it is observed that nearly the same boresight path is followed for each experiment. This is due to the corrective action of the feedback controller, which allows the nominal attitude trajectory to be reproduced despite the uncertainty in the gimbal states. Figure 10b shows that although the singularity index can vary significantly as the CMG gimbals are commanded off of their nominal trajectories, the variations are maintained above the design threshold $\mathcal{S}_{\min} = 0.45$. This ensures that sufficient control authority is retained for feedback.

V.   Conclusions

This note presents a new approach for designing shortest-time maneuvers to enhance the agility of an imaging satellite using CMGs. The maneuvers can be implemented using conventional attitude control architectures and without the need to change the flight hardware. Because standard optimal control solutions provide open-loop controls based on a nominal model of the plant, feedback is needed to implement shortest-time maneuvers in an operational setting. However, when implemented in the closed loop, unpredictable interactions between the nominal open-loop controls and the feedback law can cause the system to fail to perform as expected. To eliminate this issue, a Riemann–Stieltjes optimal control problem with a tychastic constraint can be solved instead. The proposed tychastic constraint ensures that off-nominal variations in the CMG singularity index, which occur due to feedback, can be properly managed so that control authority for feedback can be retained above a specified threshold. Experimental implementation on Honeywell's momentum control systems testbed verified that Riemann–Stieltjes optimal control solutions can be successfully implemented in a gourd test environment with real CMG hardware in the loop.

References

[1] Karpenko, M., Bhatt, S., Bedrossian, N., and Ross, I. M., "Flight Implementation of Shortest-Time Maneuvers for Imaging Satellites," *Journal of Guidance, Control, and Dynamics*, Vol. 37, No. 4, 2014, pp. 1069–1079.
doi:10.2514/1.62867

[2] McFarland, D., Swenson, E., Black, J., and Cobb, R., "Near Real-Time Closed-Loop Optimal Control Feedback for Spacecraft Attitude Maneuvers," *AIAA Modeling and Simulation Technologies Conference*, AIAA Paper 2009-5814, Aug. 2009.
doi:10.2514/6.2009-5814

[3] Ross, I. M., and Karpenko, M., "A Review of Pseudospectral Optimal Control: From Theory to Flight," *Annual Reviews in Control*, Vol. 36, No. 2, Dec. 2012, pp. 182–197.
doi:10.1016/j.arcontrol.2012.09.002

[4] Ross, I. M., *A Primer on Pontryagin's Principle in Optimal Control*, 2nd ed., Collegiate Publ., San Francisco, 2015, Chap. 1.

[5] Ross, I. M., Proulx, R. J., Karpenko, M., and Gong, Q., "Riemann–Stieltjes Optimal Control Problems for Uncertain Dynamical Systems," *Journal of Guidance, Control, and Dynamics*, Vol. 38, No. 7, 2015, pp. 1251–1263.
doi:10.2514/1.G000505

[6] Ross, I. M., Proulx, R. J., and Karpenko, M., "Unscented Optimal Control for Space Flight," *24th International Symposium on Space Flight Dynamics (ISSFD)*, John Hopkins Univ. Applied Physics Lab., Laurel, MD, May 2014, http://issfd.org/ISSFD_2014/ISSFD24_Paper_S12-5_Karpenko.pdf [retrieved 13 June 2015].

[7] Ross, I. M., Proulx, R. J., and Karpenko, M., "Unscented Optimal Control for Orbital and Proximity Operations in an Uncertain Environment: A New Zermelo Problem," *Proceedings of the AIAA/AAS Astrodynamics Specialist Conference*, AIAA Paper 2014-4423, Aug. 2014.
doi:10.2514/6.2014-4423

[8] Wie, B., *Space Vehicle Dynamics and Control*, AIAA, Reston, VA, 1998, Chap. 7.

Fig. 10   Ground test results for off-nominal CMG maneuvering using Riemann–Stieltjes optimal control: a) boresight traces; b) nominal and actual CMG singularity indices with 3σ envelope.

[9] Fleming, A., and Ross, I. M., "Singularity-Free Optimal Steering of Control Moment Gyros," *Proceedings of the AAS Astrodynamics Specialist Conference*, American Astronautical Soc. Paper 2005-418, Springfield, VA, Aug. 2005.

[10] Fleming, A., and Ross, I. M., "Minimum-Time Maneuvering of CMG-Driven Spacecraft," *Proceedings of the AAS Astrodynamics Specialist Conference*, American Astronautical Soc. Paper 2007-355, Springfield, VA, Aug. 2007.

[11] Karpenko, M., and Ross, I. M., "Implementation of Shortest-Time Maneuvers for Generic CMG Steering Laws," *Proceedings of the AIAA/ AAS Astrodynamics Specialist Conference*, AIAA Paper 2012-4959, Aug. 2012.
doi:10.2514/6.2012-4959

[12] Vadali, S. R., Walker, S. R., and Oh, H.-S., "Preferred Gimbal Angles for Single Gimbal Control Moment Gyros," *Journal of Guidance, Control, and Dynamics*, Vol. 13, No. 6, 1990, pp. 1090–1095.
doi:10.2514/3.20583

[13] McMickell, B., Buchele, P., Gisler, G., and Andrus, J., "Control Moment Gyroscope Based Momentum Control Systems in Small Satellites," U.S. Patent US8312782 B2, issued Nov. 20, 2012.